

# Direct probe of spectral inhomogeneity reveals synthetic tunability of single-nanocrystal spectral linewidths

Jian Cui, Andrew P. Beyler, Lisa F. Marshall, Ou Chen, Daniel K. Harris, Darcy D. Wanger, Xavier Brokmann and Mounqi G. Bawendi\*

**The spectral linewidth of an ensemble of fluorescent emitters is dictated by the combination of single-emitter linewidths and sample inhomogeneity. For semiconductor nanocrystals, efforts to tune ensemble linewidths for optical applications have focused primarily on eliminating sample inhomogeneities, because conventional single-molecule methods cannot reliably build accurate ensemble-level statistics for single-particle linewidths. Photon-correlation Fourier spectroscopy in solution (S-PCFS) offers a unique approach to investigating single-nanocrystal spectra with large sample statistics and high signal-to-noise ratios, without user selection bias and at fast timescales. With S-PCFS, we directly and quantitatively deconstruct the ensemble linewidth into contributions from the average single-particle linewidth and from sample inhomogeneity. We demonstrate that single-particle linewidths vary significantly from batch to batch and can be synthetically controlled. These findings delineate the synthetic challenges facing underdeveloped nanomaterials such as InP and InAs core-shell particles and introduce new avenues for the synthetic optimization of fluorescent nanoparticles.**

The past 20 years have seen great advances in synthetic control over many critical properties of colloidal semiconductor quantum dot nanocrystals, including size polydispersity<sup>1</sup>, quantum yield<sup>2</sup>, photostability<sup>3</sup> and photoluminescence intermittency<sup>4</sup>. Because of their unique and synthetically tunable optical and electronic properties, these materials have been successfully implemented in applications such as biological imaging<sup>5</sup> and solid-state lighting<sup>6</sup>, and also hold promise for other applications such as solar cells<sup>7</sup>, photodetectors<sup>8</sup> and lasers<sup>9</sup>.

However, most nanocrystal-based applications are still significantly limited in performance by the broad ensemble emission linewidth of nanocrystals at room temperature<sup>5,6</sup>. Although the peak spectral energy of a batch of nanocrystals is dictated by the average size of the particles<sup>10</sup>, its spectral breadth is dictated by a combination of sample inhomogeneity and the spectral linewidths of individual particles. To date, progress in synthesizing spectrally narrow nanocrystal batches has occurred primarily by reducing sample inhomogeneities without consideration of single-nanocrystal linewidths, largely because we have lacked the experimental tools and theoretical insight necessary to definitively determine the effects of synthesis on single-nanocrystal monochromaticity<sup>11–13</sup>.

Photon-correlation Fourier spectroscopy performed on emitters diffusing in solution (S-PCFS) offers a unique approach for investigating the spectra of single nanocrystals with large sample statistics, without user selection bias, with high signal-to-noise ratios and at timescales fast enough to avoid the spectral diffusion commonly observed in single-nanocrystal spectroscopy<sup>14</sup>. In this Article, we demonstrate that S-PCFS can be used to efficiently and reliably measure the spectral profile of the average single nanocrystal within an ensemble with statistical confidence, enabling the unambiguous characterization of the links between synthetic methodologies and single-nanocrystal spectral linewidths.

## Results

**Theoretical background of S-PCFS.** The key to S-PCFS is measuring the energy differences between photons rather than measuring their absolute energies<sup>15</sup>. When sampling an ensemble of particles freely diffusing through a small focal volume, energy differences between photons emitted by the same particle reflect the single-nanocrystal spectral profile. In contrast, photons emitted from different particles depend on the emission energies of each particle and therefore reflect the inhomogeneously broadened ensemble spectrum. Because the detection of photons originating from the same nanocrystal is statistically enhanced at timescales shorter than the particle dwell time in the focal volume, the single-particle contribution can be disentangled from the ensemble while maintaining ensemble-level statistics<sup>16</sup>.

S-PCFS experimentally implements this unique conceptual approach by combining the energy-resolving capabilities of interferometry with the time-resolving capabilities of Hanbury Brown and Twiss photon correlation analysis (Fig. 1). The interferometer converts spectral information into intensity fluctuations, which are interpreted by photon correlation analysis as the energy difference  $\zeta$  between photons as a function of the time separation  $\tau$  between them. In Fourier transform spectroscopy, the dependence of the output intensity on the interferometer path-length difference  $\delta$  gives the intensity interferogram, which is the Fourier transform of the spectrum  $s(\omega)$ , where  $\omega$  is the photon energy. Here, the dependence of the intensity cross-correlation function on  $\delta$  gives the 'PCFS interferogram'  $\tilde{g}(\delta, \tau)$ , which is the Fourier transform of the spectral correlation function  $p(\zeta, \tau)$ :

$$p(\zeta, \tau) = \left\langle \int s(\omega, t)s(\omega + \zeta, t + \tau)d\omega \right\rangle \quad (1)$$

The spectral correlation  $p(\zeta, \tau)$  can be interpreted as the distribution of energy differences  $\zeta$  for photons of temporal spacing  $\tau$ . Although

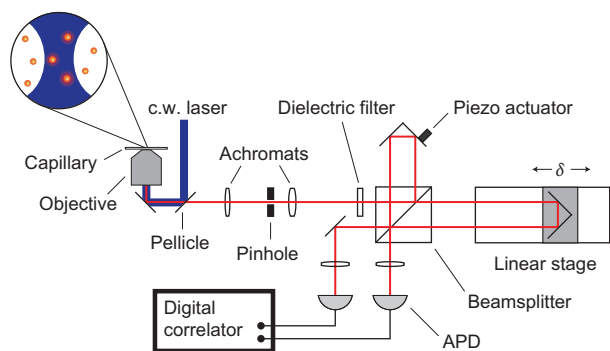


**Figure 1 | Experimental set-up.** In S-PCFS, we pass the fluorescence from particles diffusing through a small focal volume through an interferometer. With correlation analysis of the intensities at both outputs, the spectral correlation function for the average single particle can be distinguished from the spectral correlation function for the ensemble.

the spectrum itself has been sacrificed to access spectral correlations at timescales previously inaccessible to single-molecule spectroscopy, photon correlation provides the means of extracting single-emitter spectral information with ensemble-level statistics.

Traditional spectroscopy of particles diffusing in solution only provides the spectrum of the ensemble. However, encoded in  $\tilde{g}(\delta, \tau)$  are the spectral correlation functions  $p^{\text{single}}(\zeta, \tau)$  for the average single emitter and  $p^{\text{ens}}(\zeta, \tau)$  for the ensemble<sup>16,17</sup>. By analysing  $\tilde{g}(\delta, \tau)$  at timescales shorter and longer than the dwell time of the particles within the focal volume, we decompose  $\tilde{g}(\delta, \tau)$  into the contributions from the average single emitter ( $\tilde{g}^{\text{single}}(\delta, \tau)$ ) and from the ensemble ( $\tilde{g}^{\text{ens}}(\delta)$ ), which are related by a Fourier transform to their corresponding spectral correlation functions. We refer the reader to Supplementary Section S1 and refs 15–18 for more details regarding the theory and execution of this method<sup>18</sup>.

In addition to high temporal and frequency resolution, S-PCFS overcomes many of the shortcomings of traditional single-molecule spectroscopy. Assuming a single unique emitter within the focal volume at a time, a measurement of 123 intensity correlation functions with 30 s integration times for particles with an average dwell time of 300  $\mu\text{s}$  has a throughput of  $\sim 10^7$  particles with no user selection bias. Furthermore, because of the short exposure times, low-intensity continuous-wave (c.w.) excitation and a correction for fluctuations in the total signal (Supplementary Section S1), emission intermittency and bleaching are no longer experimental concerns. Finally, integration time and temporal resolution are decoupled in S-PCFS, which means that arbitrarily high signal-to-noise ratios can be obtained simply by increasing the integration time for each correlation function.

**Extracting single-nanocrystal spectral linewidths.** Although S-PCFS directly measures spectral correlation functions, additional analysis is necessary to gain insight into the underlying spectrum. Marshall *et al.* found that CdSe–CdZnS core–shell nanoparticles exhibited no appreciable spectral diffusion at submillisecond timescales approaching the lifetime of the emitters under low excitation flux and ambient conditions<sup>17</sup>. In the absence of spectral dynamics, the single-particle spectral correlation function  $p^{\text{single}}(\zeta, \tau)$  simply reduces to the energy autocorrelation of the spectrum. Thus, the breadth of the spectral correlation function reflects the breadth of the underlying spectrum. For both the single-particle and ensemble components, a broader spectral correlation  $p(\zeta, \tau)$  means a broader spectrum  $s(\omega)$ .

To obtain a quantitative spectral linewidth, we adopt a model to fit the data because, without assumptions, the spectrum cannot, mathematically, be uniquely recovered from its autocorrelation. Knowing that the single-nanocrystal spectrum at room temperature is a singly peaked, nearly symmetric function, we model the spectral lineshape using a superposition of Gaussian functions and obtain a functional

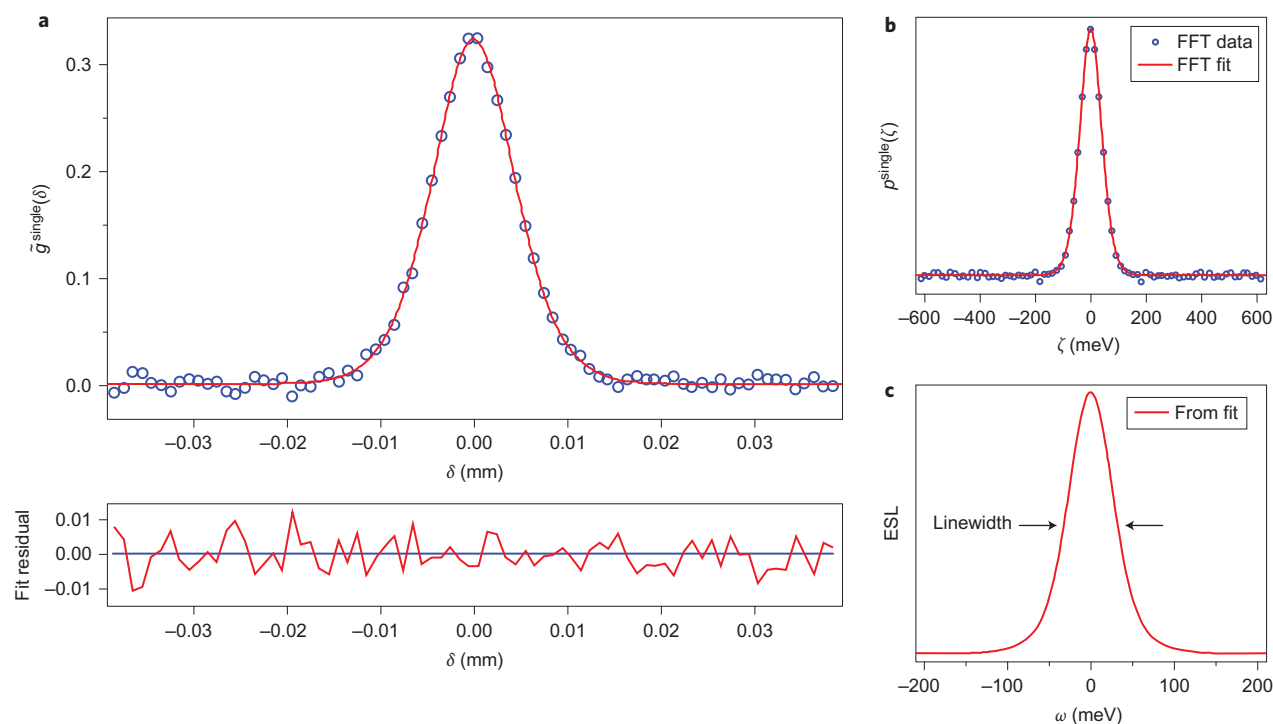


**Figure 2 | Demonstration of S-PCFS data analysis.** **a**, Single-emitter PCFS interferogram  $\tilde{g}^{\text{single}}(\delta, \tau \approx 5 \mu\text{s})$  together with fit and fitting residual. Note the high signal-to-noise ratio at a timescale more than three orders of magnitude faster than conventional methods can access. **b**, Fourier transform of  $\tilde{g}^{\text{single}}(\delta, \tau \approx 5 \mu\text{s})$  gives the spectral correlation  $p^{\text{single}}(\zeta, \tau \approx 5 \mu\text{s})$ . The good fit is conserved through the transform. **c**, The ESL is calculated from the initial fit to  $\tilde{g}^{\text{single}}(\delta, \tau \approx 5 \mu\text{s})$  and its full-width at half-maximum is the effective ‘single-nanocrystal linewidth’.

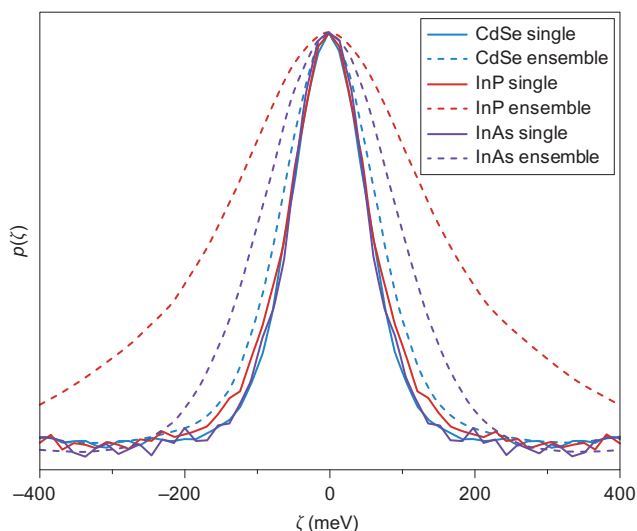


**Figure 3 | Comparison of different core materials' composition.** Single-particle (solid line) and ensemble (dotted line) spectral correlation functions  $p(\zeta, \tau \approx 5 \mu\text{s})$  for core-shell particles with CdSe (blue), InP (red) and InAs (violet) cores. Despite very different material properties and ensemble spectral linewidths, the single-nanocrystal spectral linewidths are very similar.

form to fit  $\tilde{g}^{\text{single}}(\delta, \tau)$ . An effective spectral lineshape (ESL) can be calculated from the fit and its full-width at half-maximum gives the effective 'single-nanocrystal linewidth'. The ensemble component is fit similarly. See Supplementary Sections S2 and S3 for more details and confirmation of the accuracy of our analysis.

Figure 2 provides an example of our data analysis. The measured  $\tilde{g}^{\text{single}}(\delta, \tau \approx 5 \mu\text{s})$  is plotted in blue in Fig. 2a for a batch of CdSe–CdS core-shell particles. We note the high signal-to-noise ratio at  $\tau \approx 5 \mu\text{s}$ , which is at least three orders of magnitude faster in temporal resolution than conventional single-molecule spectroscopy can achieve. Plotted in red is the fit to our model. Figure 2b shows that the fit is well-conserved to the spectral correlation  $p^{\text{single}}(\delta, \tau \approx 5 \mu\text{s})$ . The effective spectral lineshape calculated from this fit is shown in Fig. 2c.

#### Variability and tunability of single-nanocrystal linewidths.

Having demonstrated how S-PCFS can be used to measure the average single-nanocrystal spectral linewidth, we apply our method to explore the dependence of this linewidth on several nanocrystal parameters in core-shell particles. We present three experiments that illustrate how single-nanocrystal linewidths vary in ways that challenge our current understanding of the spectra of nanomaterials.

First, we investigate the effect of the core composition on the single-nanocrystal linewidth. Given that different material compositions are associated with different effective masses, dielectric constants, deformation-potential coupling and other properties that affect the materials' response to optical excitations, changing the core composition was expected to have a significant effect on the spectral linewidths<sup>19</sup>. In this experiment, we compare CdSe, InP and InAs core-shell particles. InP was chosen because it is a Cd-free alternative to CdSe, and InAs was chosen for its emission tunability into the near-infrared. These materials are of great interest for applications in displays, solid-state lighting<sup>20</sup> and biological imaging<sup>21</sup>.

In Fig. 3, we overlay the single-nanocrystal and ensemble spectral correlation functions for CdSe, InP and InAs core-shell particles. The ensemble spectral correlations confirm what is often observed in InP and InAs nanocrystals—that their ensemble spectra are much broader than those of CdSe particles<sup>22,23</sup>. Surprisingly, however, the single-nanocrystal linewidths are nearly the same. This result shows that differences in the material properties of the

core composition do not necessarily have a dramatic effect on single-nanocrystal linewidths.

In the second experiment, however, we discover large batch-to-batch variations in the average single-nanocrystal linewidths of three sample batches of commercial CdSe core-shell particles (Qdots) (Fig. 4a). Although variation in the room-temperature spectral linewidth of individual nanocrystals has been observed previously<sup>14</sup>, this is the first report of variation in the average spectral linewidth of single nanocrystals between synthetic batches. More importantly, these large single-nanocrystal linewidth variations exist despite their same core material composition (CdSe)<sup>24</sup>.

The first two experiments reveal that the core material composition does not solely dictate the single-nanocrystal linewidth, but instead, that other aspects of the core-shell architecture can have a dominant effect. We can begin to understand the structural origins of these linewidth variations through controlled synthesis in conjunction with S-PCFS.

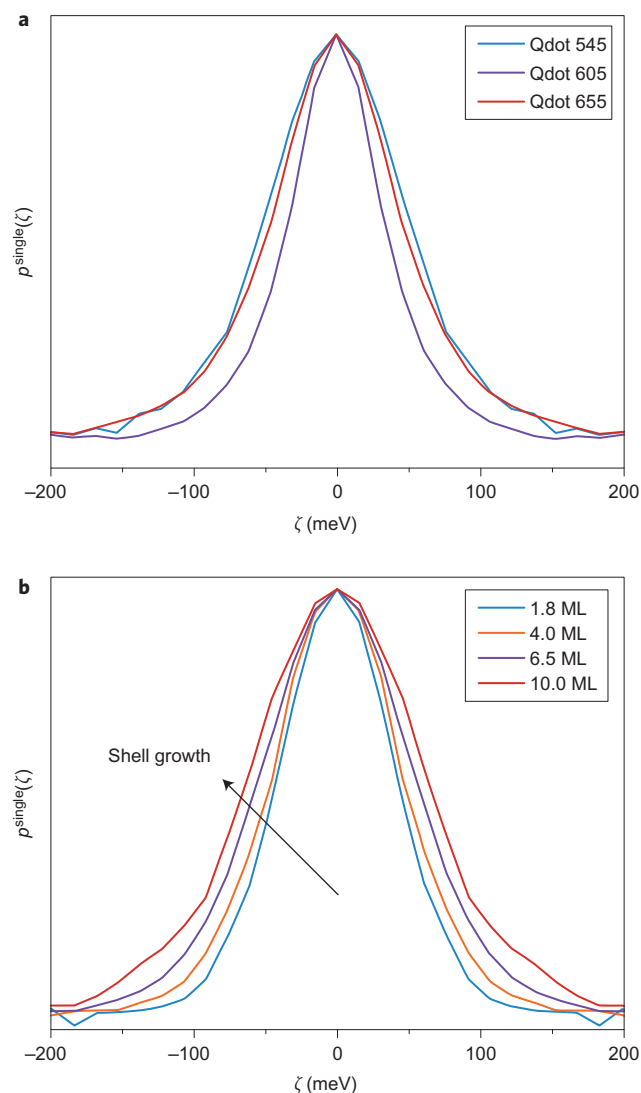


**Figure 4 | Comparison of samples with CdSe cores.** **a**, Single-particle spectral correlation functions  $p^{\text{single}}(\zeta, \tau \approx 5 \mu\text{s})$  for the commercial CdSe particles (Qdots). There is great variation in the linewidths, with no obvious trend according to size or shell morphology. **b**, Single-particle spectral correlation function  $p^{\text{single}}(\zeta, \tau \approx 5 \mu\text{s})$  for the CdSe–CdS core-shell particles during shell growth. The linewidth increases monotonically with shell growth (ML, monolayer).

In our third and final experiment, we demonstrate that the single-nanocrystal linewidth can be altered considerably by the adjustment of a synthetically controllable structural parameter. In Fig. 4b, we observe that the single-nanocrystal linewidth increases substantially for CdSe–CdS particles undergoing shell growth. In fact, Table 1 shows that the single-nanocrystal linewidth increases monotonically from 64 meV (1.8 monolayers) to an astonishing 92 meV (10 monolayers). This result does not necessarily imply that all single-nanocrystal linewidth variations, such as those observed in the second experiment, are caused by differences in shell thickness. Rather, it provides one instance in which the single-nanocrystal linewidth can be strongly influenced by structural features of the core–shell particles. This experiment brings to light the feasibility of synthetic control over single-nanocrystal linewidths.

## Discussion

Our findings have far-reaching implications for our understanding of the spectra of both single nanocrystals and nanocrystal ensembles. First, and most importantly, we have shown that the room-temperature single-nanocrystal linewidth varies considerably from batch to batch in a synthetically controllable fashion (Fig. 4). In fact, the broadest single-nanocrystal linewidth measured for the CdSe–CdS particles is even broader than the ensemble linewidth for several of the other CdSe particles (Table 1). Furthermore, single-nanocrystal linewidth synthetic tunability should be possible for nanoparticles with cores other than CdSe, because the single-nanocrystal linewidth is not dictated solely by the core composition; other aspects of the core–shell architecture can greatly alter the single-nanocrystal linewidth.

The direct consequence of these results is that the effect of the single-nanocrystal linewidth on the ensemble spectral linewidth cannot be ignored. Throughout the literature, changes in the ensemble spectral linewidth have often been attributed to changes in the size distribution of the particles<sup>22</sup>. However, our third experiment demonstrates that this conclusion is unwarranted. In the case of our CdSe particles undergoing CdS shell growth, the increase in ensemble linewidth is due primarily to broadening of the single-nanocrystal linewidth (Table 1).

Conversely, it has been speculated that the broad ensemble spectral linewidths of InP and InAs core–shell particles may be dictated by broad single-nanocrystal linewidths rather than by sample inhomogeneities. Figure 3 and Table 1 reveal that the dramatically different ensemble spectral linewidths belie nearly identical single-nanocrystal spectra. The broad ensemble spectra of InP and InAs core–shell particles are limited not by the intrinsic properties of these materials, but rather by the inhomogeneities among the particles in the sample. Thus, the synthesis of InP and InAs core–shell particles with ensemble spectral linewidths as narrow as CdSe should be achievable through the reduction of sample inhomogeneities.

These insights could not have been conclusively drawn using traditional characterization tools. A comparison of Table 1 and Supplementary Fig. S2 shows that both single-nanocrystal and ensemble spectral linewidths have little correlation with shell morphology in core–shell particles. Because transmission electron microscopy (TEM) cannot easily resolve the core from the shell, and because it relies on single-particle examination, it cannot provide an ideal measure of the degree of inhomogeneity within a synthetic batch. S-PCFS, on the other hand, provides a quantitative comparison of the single-nanocrystal and ensemble linewidths and is thus a direct probe of the degree of spectral inhomogeneity within a sample. This technique has allowed us to conclude that single-nanocrystal linewidths and sample polydispersity are independent and synthetically controllable parameters.

Finally, the single-nanocrystal linewidth variations that we observe challenge our current understanding of the physical origin of single-nanocrystal emission spectra. The breadth of the single-emitter spectrum originates from broadening of the lifetime-limited natural

**Table 1 | Single-nanocrystal and ensemble effective spectral linewidths.**

Sample	Single-nanocrystal linewidth (meV)	Ensemble linewidth (meV)
Qdot 545	70	138
Qdot 605	42	75
Qdot 655	60	90
InP core–shell	73	178
InAs–ZnS	76	151
CdSe–CdS 1.8 ML*	64	87
CdSe–CdS 4.0 ML†	69	84
CdSe/CdS 6.5 ML	82	102
CdSe/CdS 10.0 ML	92	124

ML, monolayer.

\*This sample is included in Fig. 2.

†This sample is included in Fig. 3.

emission spectrum by intrinsic and extrinsic interactions with the environment<sup>25</sup>. In the context of nanocrystals, the single-nanocrystal linewidth is believed to arise from a combination of photoinduced spectral diffusion (extrinsic) and exciton–phonon interactions (intrinsic)<sup>26</sup>. However, spectral diffusion has been found to be negligible in core–shell particles at the timescales investigated in the present work<sup>17</sup>. Thus, our results directly reflect the intrinsic single-nanocrystal spectral broadening mechanisms such as excitonic coupling to phonons within the nanoparticle<sup>27,28</sup>, to vibrations in the ligands on the surface, and to the bath solvent itself<sup>29,30</sup>.

The single-nanocrystal linewidth broadening with shell growth observed in the CdSe–CdS particles is consistent with an increased ‘Frölich-like’ exciton–phonon interaction due to the spatial separation between the electron and hole in these quasi-type-II heterostructures<sup>31,32</sup>. Our results suggest that the batch-to-batch variations in single-nanocrystal emission linewidths measured by S-PCFS originate from a delicate interplay between various parameters that affect exciton–phonon interactions within the core–shell–ligand architecture.

## Conclusions

In this Article, we have demonstrated that S-PCFS enables the simultaneous characterization of ensemble and single-emitter spectral properties with unprecedented clarity. With this new class of single-molecule spectroscopy, we have discovered batch-to-batch variability and synthetic tunability in room-temperature single-nanocrystal emission linewidths. Our work highlights the fundamental importance of the single-nanocrystal spectral linewidth when characterizing and optimizing nanocrystals for applications. With the use of S-PCFS as a high-throughput characterization tool, synthetic chemists can rapidly and quantitatively assess synthetic methodologies for the rational design of future nanostructures. In fact, our technique is already being used to help develop a new generation of nanoparticles with superior optical properties<sup>33</sup>.

We also emphasize the broad applicability of S-PCFS. Coupled with the rich and unexplored physics now accessible by our method, we anticipate that S-PCFS may serve as a platform for new perspectives on the synthesis of nanomaterials of exceptional quality. Finally, we note that although our efforts have focused on semiconductor core–shell nanoparticles, our method can be easily extended to characterize the inhomogeneities in and to probe the underlying physics of myriad fluorescent systems.

## Methods

**Experimental details.** Each sample was prepared by diluting a concentrated stock solution into a hexanes solution containing excess cadmium oleate and decylamine, which helped prevent aggregation. A thin flat capillary tube containing a dilute solution of the nanocrystal sample was mounted onto a water-immersion objective. A c.w. laser at 457 nm was used in conjunction with a pellicle beamsplitter and a dielectric notch or long-pass filter in order to achieve sensitivity across the visible spectrum.

Photoluminescence emission was collected through the same objective and focused through a pinhole to obtain a well-defined focal volume as in fluorescence correlation spectroscopy (FCS)<sup>34</sup>. The beam was recollimated and directed to a two-output Michelson interferometer. In the interferometer, the beam was split, sent to two orthogonal paths, recombined at the beamsplitter and focused onto two single-photon-counting modules (PerkinElmer, now Excelitas Technologies). On one arm of the interferometer, a retroreflector was mounted on a linear stage that defined the path-length difference  $\delta$ . On the other arm was a retroreflector mounted with a piezoelectric actuator that translated it back and forth over short distances ('dithering'). Correlation functions were obtained through a digital correlator (ALV-7004/FAST).

Each S-PCFS experiment consisted of 123 correlation measurements over 81 path-length differences. Each step of the linear stage increased the path-length difference  $\delta$  by 1  $\mu\text{m}$ , thus covering path-length differences from  $-40 \mu\text{m}$  to  $+40 \mu\text{m}$ . The path-length differences selected for these measurements provided sufficient spectral resolution for all samples measured here. The instrument function of the interferometer was less than 15  $\mu\text{eV}$ .

The centre 21 positions were measured three times and the correlation function values were averaged after correcting for diffusion and the ensemble spectral correlation. The ensemble component was selected at  $\tau \approx 100 \text{ ms}$ , a timescale much longer than the average particle dwell time in the focal volume. The PCFS interferogram  $\bar{g}^{\text{single}}(\delta, \tau)$  was then averaged over  $\tau = 1-10 \mu\text{s}$  and reported as  $\tau \approx 5 \mu\text{s}$ . The piezo actuator, receiving an input from a function generator, translated the mirror over a distance of approximately two emission wavelengths with a frequency of 0.04 Hz or 0.06 Hz. Afterpulsing correction was performed as described in ref. 17, except no short-time fitting was performed.

TEM was performed on a JEOL 200CX General Purpose TEM operating at 120 kV and on a JEOL 2010 Advanced High Performance TEM operating at 200 kV. Ensemble fluorescence spectra were measured on a Fluoromax-3 (Horiba Jobin Yvon).

**Samples.** The synthesis of InAs–ZnS and CdSe–CdS core-shell particles is described in Supplementary Sections S5 and S6. The emission maximum of the InAs–ZnS particles was 710 nm and the emission maxima of the CdSe–CdS particles were between 600 and 620 nm.

Commercial CdSe samples Qdot 545 (SKU no. Q21791MP, lot no. 801737), Qdot 605 (SKU no. Q21701MP, lot no. 786124) and Qdot 655 (SKU no. Q21721MP, lot no. 691974) were purchased from Invitrogen (now Life Technologies). The InP sample was obtained from QD Vision.

Received 18 January 2013; accepted 16 April 2013;  
published online 2 June 2013

## References

- Murray, C. B., Norris, D. J. & Bawendi, M. G. Synthesis and characterization of nearly monodisperse CdE (E = S, Se, Te) semiconductor nanocrystallites. *J. Am. Chem. Soc.* **115**, 8706–8715 (1993).
- Greytak, A. B. *et al.* Alternating layer addition approach to CdSe/CdS core/shell quantum dots with near-unity quantum yield and high on-time fractions. *Chem. Sci.* **3**, 2028–2034 (2012).
- Hines, M. A. & Guyot-Sionnest, P. Synthesis and characterization of strongly luminescing ZnS-capped CdSe nanocrystals. *J. Phys. Chem.* **100**, 468–471 (1996).
- Wang, X. *et al.* Non-blinking semiconductor nanocrystals. *Nature* **459**, 686–689 (2009).
- Medintz, I. L., Uyeda, H. T., Goldman, E. R. & Mattoussi, H. Quantum dot bioconjugates for imaging, labelling and sensing. *Nature Mater.* **4**, 435–446 (2005).
- Steckel, J. S. *et al.* Color-saturated green-emitting QD-LEDs. *Angew. Chem. Int. Ed.* **45**, 5796–5799 (2006).
- Tang, J. & Sargent, E. H. Infrared colloidal quantum dots for photovoltaics: fundamentals and recent progress. *Adv. Mater.* **23**, 12–29 (2011).
- Konstantatos, G. *et al.* Ultrasensitive solution-cast quantum dot photodetectors. *Nature* **442**, 180–183 (2006).
- Eisler, H.-J. *et al.* Color-selective semiconductor nanocrystal laser. *Appl. Phys. Lett.* **80**, 4614–4616 (2002).
- Bawendi, M. G., Steigerwald, M. L. & Brus, L. E. The quantum mechanics of larger semiconductor clusters ('quantum dots'). *Annu. Rev. Phys. Chem.* **41**, 477–496 (1990).
- Moerner, W. E. & Fromm, D. P. Methods of single-molecule fluorescence spectroscopy and microscopy. *Rev. Sci. Instrum.* **74**, 3597–3619 (2003).
- Empedocles, S. A., Neuhauser, R., Shimizu, K. T. & Bawendi, M. G. Photoluminescence from single semiconductor nanostructures. *Adv. Mater.* **11**, 1243–1256 (1999).
- Gómez, D. E., Califano, M. & Mulvaney, P. Optical properties of single semiconductor nanocrystals. *Phys. Chem. Chem. Phys.* **8**, 4989–5011 (2006).
- Gómez, D. E., van Embden, J. & Mulvaney, P. Spectral diffusion of single semiconductor nanocrystals: The influence of the dielectric environment. *Appl. Phys. Lett.* **88**, 154106 (2006).
- Brokmann, X., Bawendi, M., Coolen, L. & Hermier, J.-P. Photon-correlation Fourier spectroscopy. *Opt. Express* **14**, 6333–6341 (2006).
- Brokmann, X., Marshall, L. F. & Bawendi, M. G. Revealing single emitter spectral dynamics from intensity correlations in an ensemble fluorescence spectrum. *Opt. Express* **17**, 4509–4517 (2009).
- Marshall, L. F., Cui, J., Brokmann, X. & Bawendi, M. G. Extracting spectral dynamics from single chromophores in solution. *Phys. Rev. Lett.* **105**, 053005 (2010).
- Coolen, L., Brokmann, X., Spinicelli, P. & Hermier, J.-P. Emission characterization of a single CdSe–ZnS nanocrystal with high temporal and spectral resolution by photon-correlation Fourier spectroscopy. *Phys. Rev. Lett.* **100**, 027403 (2008).
- Banin, U., Cerullo, G., Guzelian, A. & Bardeen, C. Quantum confinement and ultrafast dephasing dynamics in InP nanocrystals. *Phys. Rev. B* **55**, 7059–7067 (1997).
- Kim, S. *et al.* Highly luminescent InP/GaP/ZnS nanocrystals and their application to white light-emitting diodes. *J. Am. Chem. Soc.* **134**, 3804–3809 (2012).
- Allen, P. M. *et al.* InAs(ZnCdS) quantum dots optimized for biological imaging in the near-infrared. *J. Am. Chem. Soc.* **132**, 470–471 (2010).
- Reiss, P., Protière, M. & Li, L. Core/shell semiconductor nanocrystals. *Small* **5**, 154–168 (2009).
- Aharoni, A., Mokari, T., Popov, I. & Banin, U. Synthesis of InAs/CdSe/ZnSe core/shell1/shell2 structures with bright and stable near-infrared fluorescence. *J. Am. Chem. Soc.* **128**, 257–264 (2006).
- Johnson, I. & Spence, M. T. Z. (eds) *Molecular Probes Handbook, A Guide to Fluorescent Probes and Labeling Technologies* 11th edn (Life Technologies, 2010).
- Nguyen, D. T. *et al.* Excitonic homogeneous broadening in single-wall carbon nanotubes. *Chem. Phys.* **413**, 102–111 (2013).
- Empedocles, S. A. & Bawendi, M. G. Influence of spectral diffusion on the line shapes of single CdSe nanocrystallite quantum dots. *J. Phys. Chem. B* **103**, 1826–1830 (1999).
- Kelley, A. M. Electron–phonon coupling in CdSe nanocrystals. *J. Phys. Chem. Lett.* **1**, 1296–1300 (2010).
- Sagar, D. *et al.* Size dependent, state-resolved studies of exciton–phonon couplings in strongly confined semiconductor quantum dots. *Phys. Rev. B* **77**, 235321 (2008).
- Salvador, M. R., Hines, M. A. & Scholes, G. D. Exciton–bath coupling and inhomogeneous broadening in the optical spectroscopy of semiconductor quantum dots. *J. Chem. Phys.* **118**, 9380–9388 (2003).
- Salvador, M. R., Graham, M. W. & Scholes, G. D. Exciton–phonon coupling and disorder in the excited states of CdSe colloidal quantum dots. *J. Chem. Phys.* **125**, 184709 (2006).
- Chernikov, A. *et al.* Phonon-assisted luminescence of polar semiconductors: Fröhlich coupling versus deformation-potential scattering. *Phys. Rev. B* **85**, 035201 (2012).
- Brovelly, S. *et al.* Nano-engineered electron–hole exchange interaction controls exciton dynamics in core–shell semiconductor nanocrystals. *Nature Commun.* **2**, 280 (2011).
- Chen, O. *et al.* Compact high-quality CdSe–CdS core–shell nanocrystals with narrow emission linewidths and suppressed blinking. *Nature Mater.* **12**, 445–451 (2013).
- Haustein, E. & Schwill, P. Fluorescence correlation spectroscopy: novel variations of an established technique. *Annu. Rev. Biophys. Biomol. Struct.* **36**, 151–169 (2007).

## Acknowledgements

This work was supported by the US Department of Energy, Office of Basic Energy Sciences, Division of Materials Sciences and Engineering (award no. DE-FG02-07ER46454) and by the National Institutes of Health through the MIT Laser Biomedical Resource Center (award no. P41EB015871-26A1). J.C. acknowledges support from the National Science Foundation Graduate Research Fellowship Program. D.D.W. acknowledges support from the Fannie and John Hertz Foundation. The authors thank QD Vision for providing the InP core–shell sample and J. Cordero for help with synthesis.

## Author contributions

J.C., L.F.M., X.B. and M.G.B. conceived and designed the experiments. J.C. performed the S-PCFS experiments. O.C. and D.K.H. synthesized the CdSe–CdS and InAs–ZnS nanoparticles. D.D.W. and O.C. performed TEM. J.C. and A.P.B. analysed the data with guidance from L.F.M., X.B. and M.G.B. The manuscript was written by J.C. and A.P.B. with contributions from all authors.

## Additional information

Supplementary information is available in the [online version](#) of the paper. Reprints and permissions information is available online at [www.nature.com/reprints](http://www.nature.com/reprints). Correspondence and requests for materials should be addressed to M.G.B.

## Competing financial interests

The authors declare no competing financial interests.